# Unveiling the electrolyte effects of CO2 electroreduction to CO and H2 evolution from the interfacial pH perspective

Liu, X.

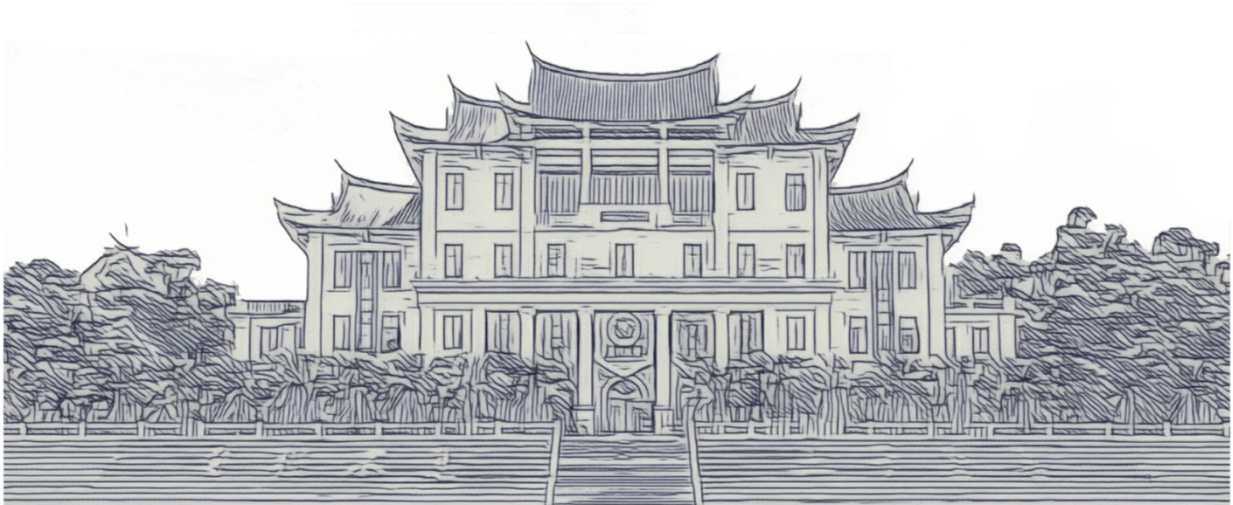

# Chapter 5

# The Effect of Weak Proton Donors on the Steady-State Behaviour of Hydrogen Evolution in Mildly Acidic Media

## Abstract

The vital importance of anionic and cationic electro-inactive species in the Hydrogen Evolution Reaction (HER) is increasingly noted. However, their influence on the steady-state current of HER is potentially underestimated. Here, the effects of these widely-used electrolyte species on the steady-state behavior of HER are investigated on a Au RDE at a bulk pH of 4. A current enhancement is observed from the coupling of proton reduction with homogeneous acid-base equilibria, with $HSO_4^-$ having the largest influence despite the electrolyte condition being far beyond its typical buffering range, while the cations, specifically $K^+$ and $Cs^+$, serve as weak buffers with limited buffer capacity. Further quantitative analysis illustrates that from the steady-state current of HER the thermodynamic parameters of the homogeneous reactions can be evaluated, taking advantage of the linear dependence of the Koutecký-Levich Slope on the concentration of the electro-inactive species. Based on this evaluation, the pKa's of $HSO_4^-$, $K^+$ and $Cs^+$ were determined to be 2.06, 2.52 and 2.48, respectively. These results confirm the previously postulated proton-donating capability of certain (alkali) cations and show that these effects influence the HER current in mildly acidic media.

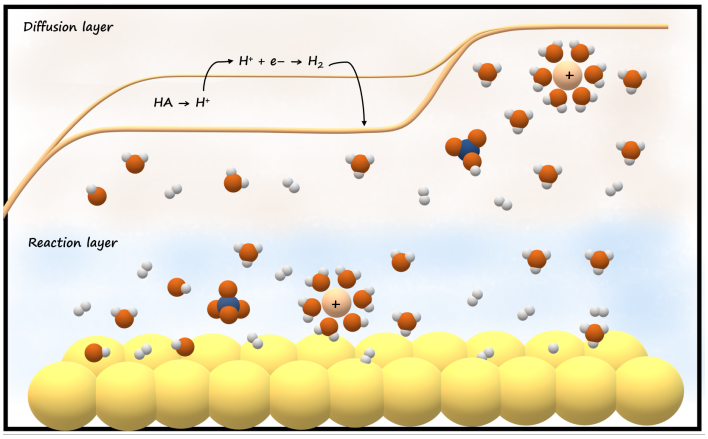


This chapter is based on Liu, X.; Koper, M. T. M., The Effect of Weak Proton Donors on the Steady-State Behavior of Hydrogen Evolution in Mildly Acidic Media (submitted).

## 5.1 Introduction

Hydrogen is one of the most promising alternatives to fossil fuels in the pursuit of a clean and sustainable society. The Hydrogen Evolution Reaction (HER) coupled with renewable electricity, producing hydrogen from the aqueous solutions with net zero greenhouse gas emissions, is considered as the most viable avenue towards a green hydrogen future.[1-2] Furthermore, HER often competes and interacts with other electrochemical processes e.g. $CO_2$ electroreduction, [3-4] and metal electrodeposition. [5-6] High HER rates heavily impact the interfacial electrolyte properties, especially local pH and other local ion concentrations . [7-8] To control the interference from mass transport and suppress the influence of gas bubble formation, HER studies are commonly performed using a Rotating Disk Electrode (RDE). Several studies have been dedicated to interpreting the HER behavior in different electrolyte conditions. [9-11] It is well-established that a typical HER process in acidic media consists of a proton reduction regime, and a proton mass transport-limited plateau followed by a water reduction regime at more negative potentials. In the first regime, the hydronium cation is the prevailing proton source, while the water molecule provides the protons in the water reduction regime (Eqs. 1-2): [12]

$$2\mathrm{H}^+ + 2\mathrm{e}^- \leftrightarrow \mathrm{H}_2 \quad (1)$$

$$2\mathrm{H}_2\mathrm{O} + 2\mathrm{e}^- \leftrightarrow \mathrm{H}_2 + 2\mathrm{OH}^- \quad (2)$$

The proton reduction current is expected to be first order in proton concentration, while water reduction current has a complicated dependence on local pH, local cation concentration, and mass transport.[13] The limiting current density due to proton reduction can be calculated according to the Levich Equation (Eq. 3): [14-15]

$$i_l = 0.62nFAD_H^{2/3}\omega^{1/2}\upsilon^{-1/6}C_H \quad (3)$$

where $n$ is the electron transfer number per proton (1 for HER here), $F$ is the Faraday constant, $D_H$ is the diffusion coefficient of the proton ($cm^2\ s^{-1}$), $\omega$ is the angular rotation rate ($rad\ s^{-1}$), $\upsilon$ is the kinematic viscosity ($cm^2\ s^{-1}$), $C_H$ is the bulk concentration of the proton. This equation is often used to obtain the diffusion coefficient of the reactive species (in this case proton) in the electrolyte under study.

Importantly, special care must be taken to ascertain the applicability of the Levich equation under particular circumstances. The assumptions involved in the derivation of the Levich equation impose limitations on its applicability to those reactions with a low concentration of supporting electrolyte and those coupled with homogeneous reactions. [16-17] Specifically, so-called electro-inactive species, which do not participate directly in the heterogeneous electron-transfer reaction, can play an important role in the steady-state current of HER. The first role is *via* electromigration, when the concentration of supporting electrolyte is not appreciably larger than the bulk proton concentration. Such a situation gives rise to a

migration contribution to mass transport. [18-19] As reported by Osteryoung et al, [20-21] the steady-state current density without supporting electrolyte is two times larger than that with excess supporting electrolyte. Amatore et al[18] also addressed this effect with an analytical model to quantify the migration effects on the steady-state current density.

Of interest in this work is a second effect by which electro-inactive species may modify the steady-state behavior of HER, namely through a preceding chemical reaction, specifically an acid-base reaction, which alters the reactive flux by generating protons. Such a mechanism is referred to as a CE process (Eqs. 4-5): [22-23]

$$HA \leftrightarrow H^+ + A^- \qquad \text{C Step} \tag{4}$$

$$2H^+ + 2e^- \leftrightarrow H_2 \qquad \text{E Step} \tag{5}$$

By postulating that the reaction layer (in which the chemical reaction C is disturbed by the interfacial E step) is thinner than the diffusion layer, Koutecký and Levich could deconvolute the chemical reaction from the mass transport. The equation for the steady-state current of the CE process is obtained by assuming that all species have equal diffusion coefficients ($i_{KL}$, Eq. 6), [24]

$$i_{KL} = \frac{FD\left(C_{HA}^b + C_H^b\right)}{\delta_D + K\sqrt{\frac{D}{k_f + k_b}}} \tag{6}$$

where *D* denotes the diffusion coefficient of the proton and the proton donors, $\delta_D$ signifies the thicknesss of the diffusion layer, $C_X^b$ is the bulk concentration of *X* species, *K* is the equilibrium constant of Eq. 4, and $k_f$ and $k_b$ are the rate constants of the forward and backward reaction of Eq. 4. Later, Dogonadze[25] extended this equation to the case of unequal diffusion coefficients ($i_{DG}$, Eq. 7).

$$i_{DG} = \frac{F\frac{D_H k_f + D_{HA} k_b}{k_f + k_b}\left(C_{HA}^b + C_H^b\right)}{\delta_D \sqrt[3]{\frac{D_H k_f + D_{HA} k_b}{D_{HA}(k_f + k_b)}} + K\frac{D_H}{D_{HA}}\sqrt{\frac{D_{HA} D_H}{D_H k_f + D_{HA} k_b}}} \tag{7}$$

There are also numerical studies to simulate the steady-state behavior of the CE process on RDEs[26-27]. Rebouillat et al[22] developed a mathematical simplification of the original Koutecký-Levich equation (Eq. 6) for different rate-limiting scenarios, dependent on the competition between the chemical reaction kinetics and diffusion. Specifically, when the reaction rate is still controlled by diffusion but modified by the preceding homogeneous process, the steady-state current is evaluated through Eq. 8,

$$\frac{1}{i} = \frac{\omega^{-1/2}}{0.62nFAD_{HA}^{2/3}\upsilon^{-1/6}KC_\Sigma} \tag{8}$$

where $C_\Sigma$ is the total concentration of the proton donors. These equations have been used to study the kinetics and thermodynamics of the HER-coupled dissociation of weak acids,

e.g. acetic acid, [28] and citric acid. [29]

Apart from these aforementioned typical acids, any conjugated acid that is capable of deprotonation in an aqueous solution may function as a potential proton donor for HER, including buffering anions and cations commonly used as supporting electrolytes. [30-32] Dating back to 1960, Cosijn [33] observed that the mono/di-hydrogen phosphate anions enhance the HER current leading to the appearance of extra current density plateaus in the polarization curves. Jackson et al. [34] also reported that phosphate can outcompete water as the primary proton source and enable HER activity at a neutral pH comparable to that at pH 1. Besides, the findings of Moreno-García et al. [35] and our previous work [36] have validated bisulfate as a proton donor. More recently, alkali metal cations in the vicinity of a negative-polarized electrode have also been suggested to be weak buffers (Eq. 9),

$$[M^+(H_2O)_n] + H_2O \rightleftharpoons H_3O^+ + [MOH(H_2O)_{n-1}] \quad (9)$$

with a buffering capability decreasing in the order $Cs^+ > Rb^+ > K^+ > Na^+ > Li^+$. A computational study by Singh et al. [37] indicated that the interaction between the negative charge on the electrode and the alkali cations facilitates the hydrolysis of the water molecules from the cation's hydration shell, thereby decreasing the $pK_a$ of the cations. In-situ pH measurements also confirmed the decrease of local pH due to the presence of weakly hydrated cations such as $K^+$ and $Cs^+$. [38-40]

A comprehensive understanding of the interfacial reaction processes includes probing the vital roles that the electro-inactive species play in heterogeneous charge transfer reactions. [41-42]. In this work, we studied the HER performance in different electrolyte conditions on a Au-RDE in order to distinguish the effects of the aforementioned (weak) proton donors, namely the bisulfate anion and the alkali cations, on the HER behavior. To highlight exclusively the implicit influence of these species, the bulk pH was meticulously maintained at 4 to suppress the impact from the bulk protons. The total electrolyte concentration was controlled to suppress any interference from electromigration. We show that HER is still under mass transport control but modified by the homogenous reaction process. Importantly, the current enhancement contributed by the protons generated from the dissociation of the protic anion ($HSO_4^-$) and the hydrolysis of alkali cations near the electrode interface can be quantified and the corresponding equilibrium constant *K* can be evaluated.

## 5.2 Experimental section

**Materials and Chemicals.** Ultrapure water (>18.2 MΩ cm, Millipore Milli-Q) and the following chemicals were used to prepare electrolytes involved in the measurements: $LiClO_4$ (>99.99%, trace metal basis, Sigma-Aldrich), $NaClO_4$ (>99.99%, trace metal basis, Sigma-

Aldrich), $KClO_4$ (>99.99%, trace metal basis, Sigma-Aldrich), $Li_2SO_4$ (>99.99%, trace metal basis, Sigma-Aldrich), $Na_2SO_4$ (99.99% Suprapur, Sigma-Aldrich), $K_2SO_4$ (>99.99%, Suprapur, Sigma-Aldrich), and $H_2SO_4$ (96% Suprapur, Merck). The pH of the electrolytes was adjusted by $H_2SO_4$ (96% Suprapur, Merck) and $HClO_4$ (70% Suprapur, Merck,) and measured by a glass-electrode pH meter (Lab 855, SI Analytics) calibrated with standard buffer solutions (Radiometer Analytical), then deaerated by a Ar purge (6.0 purity, Linde, 20 min) prior to experiments. All the electrochemical experiments were carried out in homemade single-compartment electrochemical cells controlled by a 4-channel Biologic potentiostat (VSP-300) and a Modulated Speed Rotator (Pine Research). A three-electrode system was utilized in all the electrochemical measurements, involving a RDE tip (E5TQ ChangeDisk, PEEK Shroud, Pine Research) as the working electrode, a Au wire (0.5 mm diameter, MaTeck, 99.9%) as a counter electrode and a Ag/AgCl electrode (RE-1B, 3 M NaCl, Biologic, connected to the main chamber through a Luggin capillary) as a reference electrode.

**Preparation.** Prior to measurements, electrolytes were prepared freshly employing certain amounts of aforementioned chemicals. To meticulously control the bulk pH, the electrolytes were prepared by adding a certain amount of 0.1 M proton-donor electrolyte (bulk pH 4.0) to a certain amount 0.1 M supporting electrolyte (bulk pH 4.0). For example, the serial measurements in $LiClO_4$ + $KClO_4$ started from 0.1 M $LiClO_4$ (bulk pH 4.0), then 5 mL 0.1 M $KClO_4$ (bulk pH 4.0) was added to 95 mL of the previous electrolyte (i.e. 0.1 M $LiClO_4$) for the second measurement, and the bulk pH was remeasured by the pH meter and adjusted if any deviation from 4.0 occurred. Next, 10 mL 0.1 M $KClO_4$ (bulk pH 4.0) was added to 90 mL of the previous electrolyte (i.e. 5 mM $LiClO_4$ + 95 mM $KClO_4$) for the third measurement. Detailed compositions and the corresponding bulk pH of the electrolytes are given in the Supporting Information. The electrochemical cells and other glassware were stored in acidified $KMnO_4$ solution (1 g $L^{-1}$ $KMnO_4$ in 0.5 M $H_2SO_4$) overnight and then immersed in dilute piranha to remove the generated $MnO_x$ and the residual $KMnO_4$, followed rinsing and boiling in ultrapure water for five times. The RDE tip was polished with the 3 µm, 1 µm, 0.25 µm diamond suspension (MetaDi, Buehler) respectively, with the Au disk (r = 5mm) embedded in the PEEK shroud and sonicated in ethanol and ultrapure water for 5 min in between each step.

**Electrochemical measurements.** Prior to measurements, the Au RDE tip was electropolished in 0.1 M $H_2SO_4$ (Ar-saturated) by cycling between 0 and 1.75 V vs RHE at 500 mV $s^{-1}$ for 200 times, followed by a characterizing cyclic voltammogram under the same conditions at 100 m V $s^{-1}$ on Au, to examine the surface and calculate the electrochemical surface area (ECSA) by dividing the charge of the Au oxide reduction peak with the charge density of a Au oxide monolayer (386 µC $cm^{-2}$). The Ar flow was kept purging into the

electrolyte during the measurements to avoid any interference from oxygen. The solution resistance was determined by electrochemical impedance spectroscopy (EIS) and the electrode potential was compensated for 85% of the ohmic drop. Details of quantitative analysis are explained in the Supporting Information.

## 5.3 Results and discussion

The HER performance in sulfate solutions was investigated on a Au RDE with a bulk pH of 4.0. As illustrated in Figure 1, the polarization curves show two characteristic exponential regimes separated by a plateau. At low overpotential, the current is controlled (kinetically) by proton reduction. As the protons near the interface deplete with increasing polarization, the reaction rate becomes controlled by mass transport, leading to the plateau current. In the simplest case, the value of the limiting current density is proportional to the bulk proton concentration, i.e. an exclusive function of bulk pH. However, the steady-state behavior of HER in Fig.1 perceptibly varies with the cation identity and the electrolyte concentration despite the fact that the bulk pH is the same. This effect cannot be attributed to an electromigration effect as a higher ionic strength would suppress proton migration and lead to a lower current, whereas we observe the opposite. To test whether acid-base equilibria may be involved, similar measurements were carried out in perchlorate solutions. Figure 2 depicts vastly different results compared to sulfate solutions. The (limiting) current density does not depend on the electrolyte concentration in $LiClO_4$ and $NaClO_4$. Figure 2a-b show that, although $Li^+$ and $Na^+$ do not affect proton reduction, they promote water reduction. Previous studies have shown that alkali cations aid in water reduction *via* stabilization of the reaction intermediate. [43] Therefore, for the results in Fig.1, the sulfate anion must be responsible for the observed increase in limiting current density with higher electrolyte concentration of $Li_2SO_4$ and $Na_2SO_4$, which is in agreement with the results from our previous study at a bulk pH of 3.[36] The coupling of the proton reduction and the dissociation of $HSO_4^-$ results in a concentration-dependent behavior of HER in sulfate-containing electrolyte.

Compared with Figure 2a-b, the concentration of $KClO_4$ in Figure 2c is restricted up to 100 mM, due to the solubility limitations of $KClO_4$. Importantly, an evident increase in the limiting current density is observed as the concentration rises from 50 mM to 100 mM, which suggests that $K^+$ acts as a promotor for the HER current. This amplification may be evidence for a low $pK_a$ and the resultant hydrolysis of the alkali cations in the proximity of the electrode, as has been proposed by Singh et al [37] in a computational study. This is attributed to the interaction between the cation and the negatively charged electrode facilitating the hydrolysis of the water molecule from the hydration shell of the cation. The

$pK_a$ of the cation appreciably decreases and protons are released from the cation hydration shell and contribute to the current density. Of course, the buffer capacity of the alkali cations is not as remarkable as that of the commonly-used buffer species as e.g. $HCO_3^-$, $H_2PO_4^{3-}$. [36] The hydrolysis effect of the alkali cations is easily overwhelmed by the current density from proton reduction in acidic media. It is of importance to perform the measurements in the least acidic media possible in order to facilitate the observation of the influence of cation hydrolysis, while also ensuring that the change in the limiting current density is detectable. Accordingly, the observed enhancement in Figure 1a-b is attributed to the deprotonation of $HSO_4^-$ while in Figure 1c is due to the combined effect of the deprotonation of $HSO_4^-$ and the hydrolysis of $K^+$, which explains the larger enhancement in

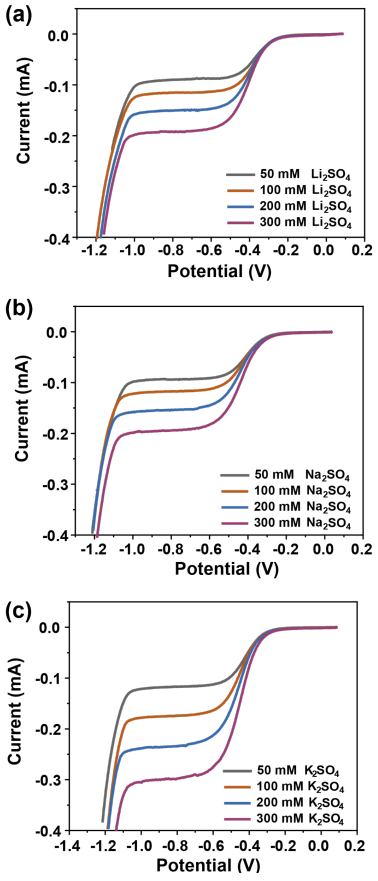


**Figure 1**. Polarization curves recorded on a Au RDE in Ar-saturated sulfate electrolytes with different cation identity and electrolyte concentration with a bulk pH of 4 at 10 mV $s^{-1}$ and a rotation rate of 2500 rpm.

Figure 1c.

To gain further insights into the effect of these potential proton donors in the electrolyte on the steady-state behavior of HER, additional experiments were conducted in a series of perchlorate electrolytes with progressively higher $SO_4^{2-}$ contents. $LiClO_4$ was employed as a supporting electrolyte, since neither Li nor $ClO_4^-$ impacts the HER behavior under these conditions, as shown in Fig.2. The total anion concentration was kept constant. As depicted in Figure 3a, the limiting current density observed increases by a factor of two relative to the pure $LiClO_4$ electrolyte, as a result of a larger proton flux provided by the $HSO_4^-$ dissociation. The linear relationships between the inverse current density and the inverse

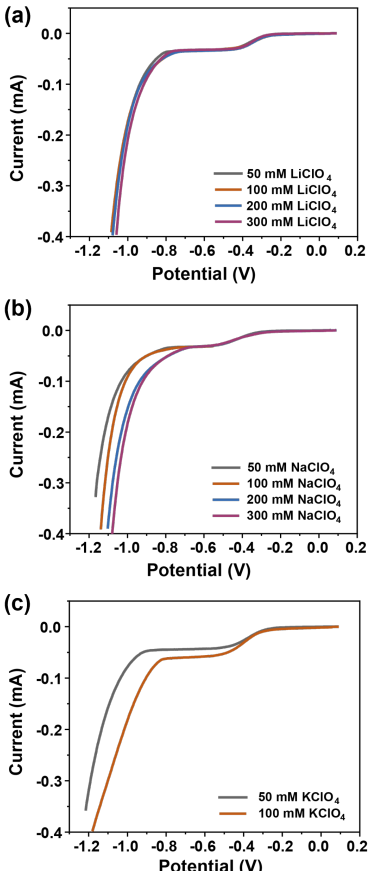


**Figure 2**. Polarization curves recorded on a Au RDE in Ar-saturated perchlorate electrolytes with different cation identity and electrolyte concentration with a bulk pH of 4 at 10 mV $s^{-1}$ and a rotation rate of 2500 rpm.

of the square root of the disk rotation rate ($\omega^{-1/2}$) shown in Figure 3b confirms that the HER rate is still controlled by diffusion, albeit impacted by the $HSO_4^-$ dissociation process. However, this diffusion control is modified by the chemical reaction as evidenced by the Koutecký- Levich slope (referred to as "$S_{K\text{-}L}$") being linearly dependent on the $SO_4^{2-}$ concentration (Fig.3c), as expressed in Eq. 10:

$$S_{K-L}{}^{-1} = 0.13\,[SO_4^{2-}]_\Sigma + 7.46 \times 10^{-6} \quad (10)$$

According to the equation proposed by Rebouillat et al. (see Eq.8 in the Introduction), [22] the equilibrium constant K can be obtained from this slope. However, since the concentration of the weak acid is assumed to be much greater than that of the proton concentration in the original analysis by Rebouillat, the current contribution from the bulk protons is neglected in the model, which is not the case in our scenario. As there is a non-zero bulk concentration of protons, the total current must be given by the sum of the direct proton reduction and the "indirect" proton reduction generated by the CE mechanism as displayed in Eqs. 11-12:

$$\frac{1}{i} = \frac{\omega^{-1/2}}{0.62nFAD_{HA}^{2/3}\upsilon^{-1/6}KC_\Sigma + 0.62nFAD_H^{2/3}\upsilon^{-1/6}C_H} \quad (11)$$

$$S_{K-L}{}^{-1} = 0.62nFAD_{HA}^{2/3}\upsilon^{-1/6}KC_\Sigma + 0.62nFAD_H^{2/3}\upsilon^{-1/6}C_H \quad (12)$$

where *n* is the electron transfer number per proton (1 for HER here), *F* is the Faraday constant, $D_{HA}$ is the diffusion coefficient of the proton donor ($cm^2\ s^{-1}$), $\omega$ is the angular rotation rate (rad $s^{-1}$), $\upsilon$ is the kinematic viscosity ($cm^2\ s^{-1}$). Based on the linear correlation between $S_{K\text{-}L}{}^{-1}$ and $SO_4^{2-}$ concentration, the $pK_a$ of $HSO_4^-$is evaluated to be 2.06, in close agreement with the reported $pK_a$ of $HSO_4^-$ (1.99).[44] Calculation details can be found in the Supporting Information.

To validate the evaluation and the effect of the cation hydrolysis, a similar analysis was performed with different cations. Experiments were conducted in a series of electrolytes with $LiClO_4$ as the supporting electrolyte and increasing concentration of other alkali cations. The dependence of the steady-state behavior of HER on $Na^+$ concentration was examined first. However, in alignment with the results above, a barely appreciable change in the limiting current density with increasing $Na^+$ concentration was found (see Figure S8 in the supporting information), meaning that hydrated $Na^+$ is an ineffective proton donor. By comparison, Figure 4a illustrates a gradual enhancement of the limiting current density of HER with the increasing $K^+$ concentration, suggesting that hydrated $K^+$ can act as a proton donor due to hydrolysis. However, the enhancement by $K^+$ is limited compared with $HSO_4^-$, due to a larger proton-donating capacity of $HSO_4^-$ than alkali cations, which is also expressed by the fact that the $S_{K\text{-}L}{}^{-1}$ of $HSO_4^-$ is over two times larger than that of $K^+$. Quantitative analysis from the slope shown in Figure 4c gives a $pK_a$ of $K^+$ of 2.52. This cation hydrolysis is

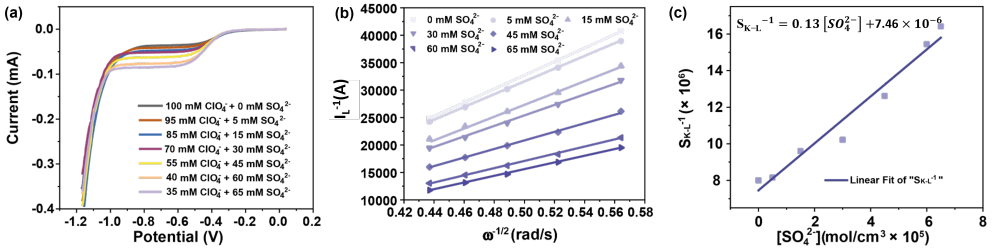


**Figure 3. a)** Polarization curves recorded on a Au RDE in Ar-saturated lithium electrolytes with a different ratio of the anion with a bulk pH of 4 at 10 mV $s^{-1}$ and a rotation rates of 2500 rpm. **b)** Koutecký-Levich plots under different electrolyte conditions from a) with the rotation rates range from 900 rpm to 2500 rpm. **c)** The correspondence between the $S_{K\text{-}L}{}^{-1}$ and the $SO_4{}^{2-}$ concentration from b) and its linear fit.

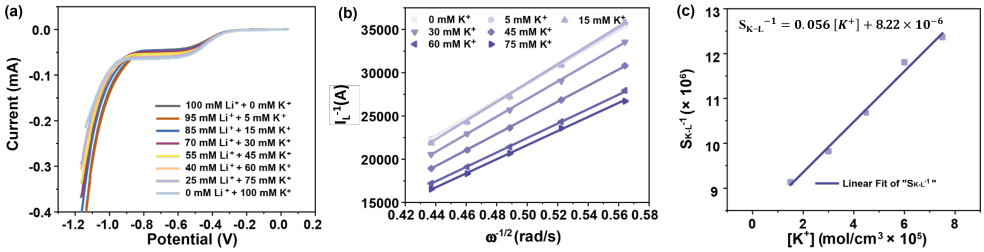


**Figure 4. a)** Polarization curves recorded on a Au RDE in Ar-saturated 100 mM perchlorate electrolytes with different ratios of cations, with a bulk pH of 4, at 10 mV $s^{-1}$ and a rotation rate of 2500 rpm. **b)** Koutecký-Levich plots for different electrolyte conditions from a) with the rotation rates ranging from 900 rpm to 2500 rpm (see experimental details in the Supporting Information). **c)** The correspondence between the $S_{K\text{-}L}{}^{-1}$ and the $K^+$ concentration from b) and its linear fit.

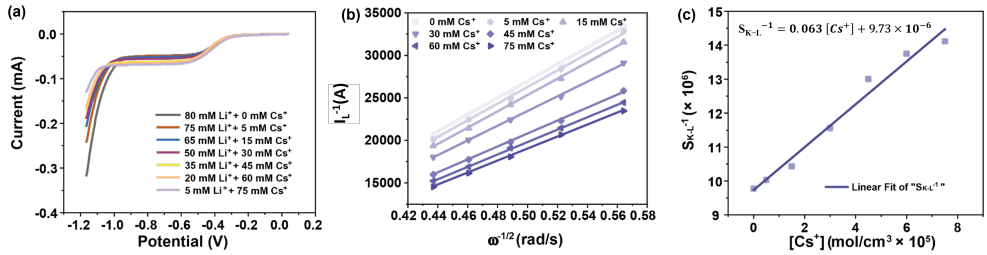


**Figure 5. a)** Polarization curves recorded on a Au RDE in Ar-saturated 100 mM perchlorate electrolytes with a different ratios of cations with a bulk pH of 4, at 10 mV $s^{-1}$ and a rotation rates of 2500 rpm. **b)** Koutecký-Levich plots for different electrolyte conditions from a) with the rotation rates ranging from 900 rpm to 2500 rpm. **c)** The correspondence between the $S_{K\text{-}L}{}^{-1}$ and the $Cs^+$ concentration from b) and its linear fit.

more pronounced than Singh et al. [37] predicted for Cu (8.49 for $K^+$, 4.32 for $Cs^+$) and Ag (7.95 for $K^+$, 4.31 for $Cs^+$) electrodes in a computational study.

Similarly, a quantitative analysis of $Cs^+$ hydrolysis is shown in Figure 5. The $Cs^+$ concentration is always below 80 mM due to the limited solubility of $Cs^+$. A greater increase in the limiting current density and a corresponding larger slope of 0.063 compared to that of $K^+$ are observed, showing that hydrated $Cs^+$ is a slightly better proton donor than $K^+$. The $pK_a$ of $Cs^+$ is determined to be 2.48.

The quantitative investigation in terms of the sulfate electrolyte is carried out involving $Li_2SO_4$ as a supporting component. In this case the limiting current density of HER is

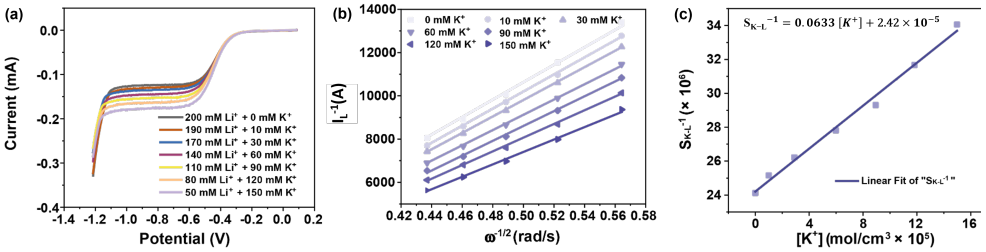


**Figure 6. a)** Polarization curves recorded on a Au RDE in Ar-saturated 100 mM sulfate electrolytes with a different ratios of cation concentrations with a bulk pH of 4, at 10 mV $s^{-1}$ and a rotation rate of 2500 rpm. **b)** Koutecký-Levich plots under different electrolyte conditions from a) with the rotation rates ranging from 900 rpm to 2500 rpm. **c)** The correspondence between the $S_{K\text{-}L}^{-1}$ and the $K^+$ concentration from b) and its linear fit.

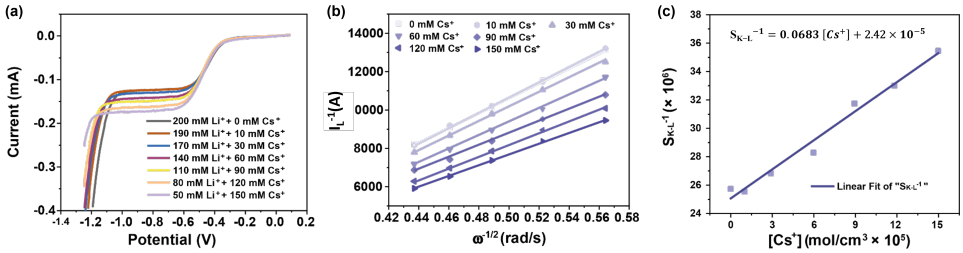


**Figure 7. a)** Polarization curves recorded on a Au RDE in Ar-saturated 100 mM sulfate electrolytes with a different ratios of cation concentrations with a bulk pH of 4, at 10 mV $s^{-1}$ and a rotation rates of 2500 rpm. **b)** Koutecký-Levich plots under different electrolyte conditions from a) with the rotation rates ranging from 900 rpm to 2500 rpm. **c)** The correspondence between the $S_{K\text{-}L}^{-1}$ and the $Cs^+$ concentration from b) and its linear fit.

contributed by the bulk protons, the dissociation of $HSO_4^-$ and the hydrolysis of the cation. The hydrated $Na^+$ is still an ineffective proton-donor in this case with a negligible change in the steady-state current response (see Figure S8 in the supporting information), while the hydrated $K^+$ and $Cs^+$ evidently enhance the limiting current density. The linear dependences between $S_{K\text{-}L}^{-1}$ and the $K^+$ and $Cs^+$ concentrations are shown in Figures 6 and 7, with a slope nearly equivalent to that in perchlorate, but an intercept twice as large. This is attributed to the additional protons from $HSO_4^-$, which is also suggested by the higher limiting current density compared to the perchlorate solution. Therefore, an additional current density was added to account for the influence from $HSO_4^-$ (Eqs. 13-14):

$$\frac{1}{i} = \frac{\omega^{-1/2}}{0.62nFAD_{cat}^{2/3}\upsilon^{-1/6}K_{cat}C_{cat}+0.62nFAD_{HSO_4^-}^{2/3}\upsilon^{-1/6}K_{HSO_4^-}C_{(H)SO_4^-}+0.62nFAD_H^{2/3}\upsilon^{-1/6}C_H} \quad (13)$$

$$S_{K-L}{}^{-1} = 0.62nFAD_{cat}^{2/3}\upsilon^{-1/6}K_{cat}C_{cat} + 0.62nFAD_H^{2/3}\upsilon^{-1/6}C_H + 0.62nFAD_{HSO_4^-}^{2/3}\upsilon^{-1/6}K_{HSO_4^-}C_{(H)SO_4^-} \quad (14)$$

The $pK_a$'s of $K^+$ and $Cs^+$ are determined to be 2.45 and 2.44, respectively, similar to the results from the values evaluated in perchlorate electrolyte. Taking the diffusion coefficient of the proton as $1.7\times10^{-4}$ $cm^2$ $s^{-1}$ as determined above, in both $K^+$ and $Cs^+$ solutions an identical value of $1.84\times10^{-5}$ $cm^2$ $s^{-1}$ is obtained for the diffusion coefficient of $HSO_4^-$, in agreement with the literature data. [44]

A similar analysis was performed in 100 mM perchlorate electrolyte with an increasing $Cs^+$ content at bulk pH 3.7 (see Figure S9 in the Supporting Information), A $S_{K\text{-}L}$ of 0.067 is obtained and the $pK_a$ of $Cs^+$ and the diffusion coefficient of the proton are evaluated to be 2.46 and $2.17\times10^{-4}$ $cm^2$ $s^{-1}$, resp. The $pK_a$ agrees well with the results obtained from measurements performed at bulk pH 4, demonstrating that this quantitative analysis is independent of bulk pH.



## 5.4 Conclusions

In this work, we investigated certain supporting electrolyte species which are also potential proton donors, and their effect on the steady-state hydrogen evolution current at a rotating disk electrode. The species studied including an anionic proton donor, i.e. bisulfate, as well as alkali cations, which have recently been suggested as proton donors in experiments of hydrogen evolution and $CO_2$ reduction.

By conducting experiments with the bulk pH kept rigorously constant, it was observed that the steady-state behavior of HER discernably varies with the concentration of the protic anion, namely $HSO_4^-$ and the alkali cation, namely $K^+$ and $Cs^+$, while the influence of $ClO_4^-$, $Li^+$ and $Na^+$ is negligible. This is related to the alteration of the reaction flux by coupling proton reduction with homogeneous acid-base equilibria, namely, dissociation of $HSO_4^-$ and hydrolysis of $K^+$ and $Cs^+$. Of these ions, $HSO_4^-$ has the biggest influence, even though the

electrolyte condition is outside its typical buffering range, while the cations serve as a weak buffer with limited capacity. Quantitative studies conducted in both perchlorate and sulfate solutions elucidated that the steady state current of HER can be modeled as a mass transport limited process coupled to a chemical reaction (i.e. the acid-base reaction). A linear variation of the Koutecký-Levich slope with respect to the concentration of electro-inactive species was observed, from which the $pK_a$ of the proton donor involved can be extracted. The corresponding $pK_a$'s of $HSO_4^-$, $K^+$ and $Cs^+$ were determined to be 2.06, 2.52 and 2.48, respectively. Specifically, these studies confirm that alkali cation species can act as proton donors and (weak) buffering agents near electrode surfaces, and that their effect can be quantified experimentally.

## References

(1)Shih, A. J.; Monteiro, M. C. O.; Dattila, F.; Pavesi, D.; Philips, M.; da Silva, A. H. M.; Vos, R. E.; Ojha, K.; Park, S.; van der Heijden, O.; Marcandalli, G.; Goyal, A.; Villalba, M.; Chen, X.; Gunasooriya, G. T. K. K.; McCrum, I.; Mom, R.; López, N.; Koper, M. T. M., Water electrolysis. *Nature Reviews Methods Primers* **2022,** *2* (1).

(2)Zou, X.; Zhang, Y., Noble metal-free hydrogen evolution catalysts for water splitting. *Chem Soc Rev* **2015,** *44* (15), 5148-80.

(3)Huang, J. E.; Li, F.; Ozden, A.; Sedighian Rasouli, A.; García de Arquer, F. P.; Liu, S.; Zhang, S.; Luo, M.; Wang, X.; Lum, Y.; Xu, Y.; Bertens, K.; Miao, R. K.; Dinh, C.-T.; Sinton, D.; Sargent, E. H., CO2 electrolysis to multicarbon products in strong acid. *Science* **2021,** *372* (6546), 1074-1078.

(4)Marcandalli, G.; Monteiro, M. C. O.; Goyal, A.; Koper, M. T. M., Electrolyte Effects on CO2 Electrochemical Reduction to CO. *Acc. Chem. Res.* **2022,** *55* (14), 1900-1911.

(5)Wu, J.; Wafula, F.; Branagan, S.; Suzuki, H.; van Eisden, J., Mechanism of cobalt bottom-up filling for advanced node interconnect metallization. *Journal of the Electrochemical Society* **2018,** *166* (1), D3136.

(6)Schlesinger, M.; Paunovic, M., *Modern electroplating*. John Wiley & Sons: 2014; Vol. 52.

(7)Monteiro, M. C. O.; Liu, X.; Hagedoorn, B. J. L.; Snabilié, D. D.; Koper, M. T. M., Interfacial pH Measurements Using a Rotating Ring-Disc Electrode with a Voltammetric pH Sensor. *ChemElectroChem* **2021,** *9* (1), e202101223.

(8)Mukouyama, Y.; Nakanishi, S., An Ordinary Differential Equation Model for Simulating Local-pH Change at Electrochemical Interfaces. *Frontiers in Energy Research* **2020,** *8*.

(9)Zhu, J.; Hu, L.; Zhao, P.; Lee, L. Y. S.; Wong, K. Y., Recent Advances in Electrocatalytic Hydrogen Evolution Using Nanoparticles. *Chem Rev* **2020,** *120* (2), 851-918.

(10)Dubouis, N.; Grimaud, A., The hydrogen evolution reaction: from material to interfacial descriptors. *Chem Sci* **2019,** *10* (40), 9165-9181.

(11)Nagel, K.; Wendler, F., Die Wasserstoffelektrode als zweifache Elektrode. *Zeitschrift für*

*Elektrochemie, Berichte der Bunsengesellschaft für physikalische Chemie* **1956,** *60* (9-10), 1064-1072.

(12)Ooka, H.; Figueiredo, M. C.; Koper, M. T. M., Competition between Hydrogen Evolution and Carbon Dioxide Reduction on Copper Electrodes in Mildly Acidic Media. *Langmuir* **2017,** *33* (37), 9307-9313.

(13)Goyal, A.; Koper, M. T. M., The Interrelated Effect of Cations and Electrolyte pH on the Hydrogen Evolution Reaction on Gold Electrodes in Alkaline Media. *Angew Chem Int Ed Engl* **2021,** *60* (24), 13452-13462.

(14)Levich, V. G.; Tobias, C. W., Physicochemical hydrodynamics. *Journal of The Electrochemical Society* **1963,** *110* (11), 251C.

(15)Bard, A. J.; Faulkner, L. R., *Electrochemical Methods: Fundamentals and Applications*. Wiley: 2012.

(16)Treimer, S.; Tang, A.; Johnson, D. C., A Consideration of the application of Koutecký-Levich plots in the diagnoses of charge-transfer mechanisms at rotated disk electrodes. *Electroanalysis* **2002,** *14* (3), 165-171.

(17)Leal, P. H. M.; Barcia, O. E.; Mattos, O. R., Numerical Analysis of CE Processes in RDE Systems: Diffusion and Electro-hydrodynamic Impedances. *Journal of The Electrochemical Society* **2020,** *167* (2), 026502.

(18)Amatore, C.; Fosset, B.; Bartelt, J.; Deakin, M.; Wightman, R., Electrochemical kinetics at microelectrodes: Part V. Migrational effects on steady or quasi-steady-state voltammograms. *Journal of electroanalytical chemistry and interfacial electrochemistry* **1988,** *256* (2), 255-268.

(19)Ciszkowska, M.; Stojek, Z.; Morris, S. E.; Osteryoung, J. G., Steady-state voltammetry of strong and weak acids with and without supporting electrolyte. *Analytical Chemistry* **1992,** *64* (20), 2372-2377.

(20)Stojek, Z.; Ciszkowska, M.; Osteryoung, J. G., Self-enhancement of voltammetric waves of weak acids in the absence of supporting electrolyte. *Analytical Chemistry* **1994,** *66* (9), 1507-1512.

(21)Jaworski, A.; Stojek, Z.; Osteryoung, J. G., A simple theoretical model for the self-enhancement of the cathodic voltammetric waves of weak acids. *Analytical Chemistry* **1995,** *67* (18), 3349-3352.

(22)Rebouillat, S.; Lyons, M. E. G.; Bannon, T., Evaluation of the proton transfer kinetics of potential electrolytes in non-aqueous solutions using electrochemical techniques Part 1. Kinetic analysis of the general CE mechanism at stationary and rotating electrodes. *J. Solid State Electrochem.* **1999,** *3* (4), 215-230.

(23)Leal, P.; Leite, N.; Viana, P.; de Sousa, F.; Barcia, O.; Mattos, O., Numerical analysis of the steady-state behavior of CE processes in rotating disk electrode systems. *Journal of The Electrochemical Society* **2018,** *165* (9), H466.

(24)Koutecky, J.; Levich, V., The use of a rotating disk electrode in the studies of electrochemical kinetics and electrolytic processes. *Zh. Fiz. Khim* **1958,** *32*, 1565-1575.

(25)Dogonadze, R., Use of Rotating Disk Electrode in the Study of the Electrochemical Kinetic and Catalytic Processes. The Case of Different Diffusion Coefficients. *Zh. Fiz. Khim.* **1958,** *32*, 2437-2442.

(26)Hale, J., Transients in convective systems: I. Theory of galvanostatic, and galvanostatic with current

reversal transients, at a rotating disc electrode. *Journal of Electroanalytical Chemistry (1959)* **1963,** *6* (3), 187-197.

(27)Compton, R.; Laing, M.; Mason, D.; Northing, R.; Unwin, P., Rotating disc electrodes: the theory of chronoamperometry and its use in mechanistic investigations. *Proceedings of the Royal Society of London. A. Mathematical and Physical Sciences* **1988,** *418* (1854), 113-154.

(28)Marinović, V.; Despić, A. R., Cathodic Hydrogen Evolution from Aqueous Solutions of Acetic Acid. *Russian Journal of Electrochemistry* **2004,** *40*, 995-999.

(29)Marinović, V.; Despić, A., Hydrogen evolution from solutions of citric acids. *Journal of Electroanalytical Chemistry* **1997,** *431* (1), 127-132.

(30)Marinović, V.; Despić, A., Pyrophosphoric acid as a source of hydrogen in cathodic hydrogen evolution on silver. *Electrochimica acta* **1999,** *44* (23), 4073-4077.

(31)Monteiro, M. C. O.; Dattila, F.; López, N.; Koper, M. T. M., The Role of Cation Acidity on the Competition between Hydrogen Evolution and CO2 Reduction on Gold Electrodes. *J. Am. Chem. Soc.* **2021,** *144* (4), 1589-1602.

(32)Marcandalli, G.; Boterman, K.; Koper, M. T. M., Understanding hydrogen evolution reaction in bicarbonate buffer. *J. Catal.* **2022,** *405*, 346-354.

(33)Cosijn, A. M., Diffusion polarisation of the hydrogen electrode: I. Theory. *Journal of Electroanalytical Chemistry (1959)* **1961,** *2* (6), 437-451.

(34)Jackson, M. N.; Jung, O.; Lamotte, H. C.; Surendranath, Y., Donor-Dependent Promotion of Interfacial Proton-Coupled Electron Transfer in Aqueous Electrocatalysis. *ACS Catal.* **2019,** *9* (4), 3737-3743.

(35)Moreno-Garcia, P.; Kovacs, N.; Grozovski, V.; Galvez-Vazquez, M. J.; Vesztergom, S.; Broekmann, P., Toward CO(2) Electroreduction under Controlled Mass Flow Conditions: A Combined Inverted RDE and Gas Chromatography Approach. *Anal Chem* **2020,** *92* (6), 4301-4308.

(36)Liu, X.; Koper, M. T. M., Tuning the Interfacial Reaction Environment for CO(2) Electroreduction to CO in Mildly Acidic Media. *J Am Chem Soc* **2024,** *146* (8), 5242-5251.

(37)Singh, M. R.; Kwon, Y.; Lum, Y.; Ager, J. W., 3rd; Bell, A. T., Hydrolysis of Electrolyte Cations Enhances the Electrochemical Reduction of CO2 over Ag and Cu. *J. Am. Chem. Soc.* **2016,** *138* (39), 13006-13012.

(38)Liu, X.; Monteiro, M. C. O.; Koper, M. T. M., Interfacial pH measurements during CO(2) reduction on gold using a rotating ring-disk electrode. *Phys. Chem. Chem. Phys.* **2023,** *25* (4), 2897-2906.

(39)Ayemoba, O.; Cuesta, A., Spectroscopic Evidence of Size-Dependent Buffering of Interfacial pH by Cation Hydrolysis during CO2 Electroreduction. *ACS Appl Mater Interfaces* **2017,** *9* (33), 27377-27382.

(40)Zhang, F.; Co, A. C., Direct evidence of local pH change and the role of alkali cation during CO2 electroreduction in aqueous media. *Angewandte Chemie International Edition* **2020,** *59* (4), 1674-1681.

(41)Kamat, G. A.; Zamora Zeledón, J. A.; Gunasooriya, G. K. K.; Dull, S. M.; Perryman, J. T.; Nørskov, J. K.; Stevens, M. B.; Jaramillo, T. F., Acid anion electrolyte effects on platinum for oxygen and hydrogen

electrocatalysis. *Communications Chemistry* **2022,** *5* (1), 20.

(42)Lu, X.; Tu, W.; Zhou, Y.; Zou, Z., Effects of electrolyte ionic species on electrocatalytic reactions: advances, challenges, and perspectives. *Advanced Energy Materials* **2023,** *13* (27), 2300628.

(43)Monteiro, M. C. O.; Goyal, A.; Moerland, P.; Koper, M. T. M., Understanding Cation Trends for Hydrogen Evolution on Platinum and Gold Electrodes in Alkaline Media. *ACS Catal* **2021,** *11* (23), 14328-14335.

(44)Lide, D. R., *CRC handbook of chemistry and physics*. CRC press: 2004; Vol. 85.